WILEY-VCH

RESEARCH ARTICLE

Electrochemically and Photochemically Induced Hydrogen Evolution Catalysis with Co-Tetraazamacrocycles Occur via Different Pathways

Sergi Grau,[a] Mauro Schilling,[b] Dooshaye Moonshiram,[a,⊥] Jordi Benet-Buchholz,[a] Sandra Luber,*[b] Antoni Llobet*[a,c] and Carolina Gimbert-Suriñach*[a]

Abstract: Cobalt complexes containing equatorial tetraazamacrocyclic ligands are active catalysts for the hydrogen evolution reaction in pure aqueous conditions. Herein we explore the effect of different groups directly linked to the macrocyclic ligand (-NH-, -NH_2^+- or –$N(CH_2OH)$-). Electrochemically induced hydrogen evolution catalysis studies at pH 4 invoke a mechanism, in which the rate determining step is the protonation of the reduced Co^I species that gives a cobalt hydride (Co^{III}-H), a key intermediate towards the H-H bond formation. In sharp contrast, under photochemical conditions using $[Ru(bpy)_3]^{2+}$ as a photosensitizer and ascorbate as sacrificial electron donor, the formation of a "Co^0" species that quickly protonates to give a Co^{II}-H is proposed. In this scenario, the rate determining step is the H-H bond formation that occurs in an intermolecular fashion from the Co^{II}-H species and a water molecule. Both mechanisms are supported by density functional theory (DFT) calculations that allowed us to estimate the pK_a values of the Co^{III}-H and Co^{II}-H species, as well as transition states based on intramolecular and intermolecular H-H bond formation from Co^{II}-H.

Introduction

The generation of hydrogen gas from light induced water splitting is a highly pursued process for its sustainable nature and high-energy storage capabilities of the hydrogen molecule.[1,2] The development of catalysts based on transition metal complexes to perform the water reduction half-reaction is an active field that has given rise to a plethora of new compounds exploiting the tunable electronic effect of the ligands and their capacity to store multiple electrons on the metal site, the ligand or both.[3–8] Another useful feature of molecular based hydrogen evolution catalysts is the possibility to include proton relay groups in the second coordination sphere of the metal, thus facilitating the H-H bond formation step by strategically locating a proton close to a metal hydride.[9]

A prominent example of a molecular hydrogen evolution catalyst is the cobalt macrocyclic complex **1** in Figure 1, which has shown remarkable stability under catalytic turnover in acidic water. This catalyst has been successfully used in electrocatalytic[10,11] as well as photocatalytic systems in combination with metal based molecular photosensitizers,[11–13] quantum dots[14,15] and organic dyes.[16] The mechanism followed by **1** was recently studied through time-resolved pump(laser)/x-ray(probe) spectroscopy with pico-microsecond time resolution under photocatalytic conditions with $[Ru(bpy)_3]^{2+}$ photosensitizer and the rate determining step of the process, involving the formation of the key Co^{III} hydride (Co^{III}-H) intermediate was determined.[13] One of the interesting features of **1** is the secondary amine group of the macrocyclic ligand that could be involved in an intramolecular H-H bond formation step, as proposed for other catalysts, including the naturally occurring hydrogenases.[9] In this work, we study the hydrogen evolution mechanism followed by cobalt complexes derived from **1** that have different substituents in the amine group and we explore their role as intramolecular proton relays. In the new complexes **2** and **3** in Figure 1, the secondary amine in **1** is substituted by a tertiary amine. In addition, for complex **3** we introduce an extra acidic group further away from the metal center, which could be potentially involved in the catalytic process.

[a] Dr. S. Grau, Dr. D. Moonshiram, Dr. J. Benet-Buchholz, Dr. C. Gimbert-Suriñach and Prof. Dr. A. Llobet
Institute of Chemical Research of Catalonia (ICIQ), Barcelona Institute of Science and Technology (BIST)
Av. Països Catalans 16, 43007, Tarragona, Spain
E-mail: cgimbert@iciq.cat, allobet@iciq.cat

[b] M. Schilling, Prof. Dr. S. Luber
Department of Chemistry
University of Zurich
Winterthurerstrasse 190, 8057 Zurich, Switzerland
E-mail: sandra.luber@chem.uzh.ch

[c] Prof. Dr. A. Llobet
Department de Química
Universitat Autònoma de Barcelona
Cerdanyola del Vallès, 08193 Barcelona, Spain

Supporting information for this article is given via a link at the end of the document. Crystallographic data of **2**-**5** can be found in CCDC 1958402-1958405.

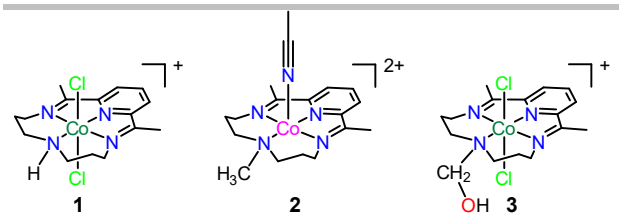

Figure 1. Cobalt hydrogen evolution catalysts investigated in this study.

Results and Discussion

Synthesis, spectroscopic and structural characterization of 2-5

Compounds **2** and **3** which have never been reported before were prepared using a synthetic procedure adapted from that described for the well-known compound **1**.[17] It consists of a one-step template synthesis starting from 2,6-diacetylpyridine and *N,N*-bis-(3-aminopropyl)-methylamine and a cobalt precursor ($Co(NO_3)_2$ or $CoCl_2$) under nitrogen atmosphere. Detailed synthetic procedures, spectroscopic and analytical characterizations are described in the experimental section. Single crystals suitable for x-ray diffraction (XRD) studies were obtained and their ORTEP plots are shown in Figure 2. Compound **2** is a Co^{II} five-coordinated complex with a distorted square-based pyramid geometry with an acetonitrile molecule occupying the axial position. This structure is analogous to that of the Co^{II} compound derived from **1**, with similar bond distances and angles.[18] On the other hand, complex **3** is a Co^{III} six-coordinated compound with two chlorido ligands in the axial positions, which has very similar bond distances to those of **1**.[11,13] The dangling alcohol in the amino group of the macrocyclic ligand in **3** is prone to coordination, generating compound **4** in Figure 2. In the presence of excess cobalt chloride, precursor in the synthetic mixture, compound **4** evolves to the dicobalt complex **5**. In the presence of hydrochloric acid, derivatives **4** evolves to catalyst **3** (Scheme S1).

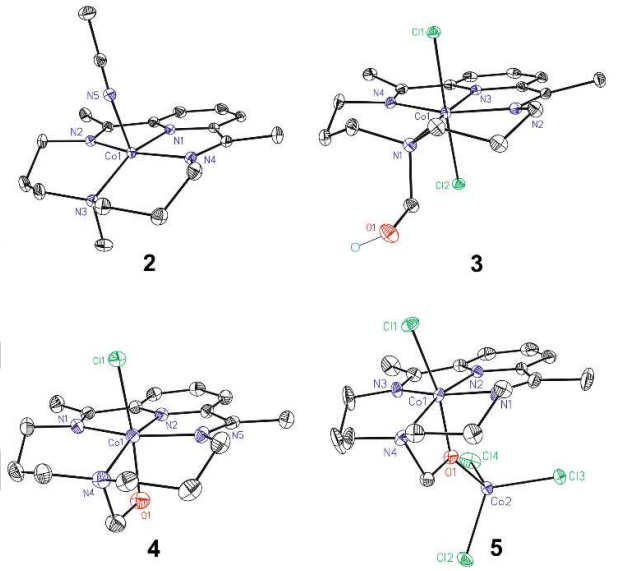

Figure 2. X-ray diffraction structures. ORTEP plots at 50% probability of cationic species **2**, **3**, **4** and neutral dinuclear complex. Only the H atom connected to hydroxomethyl group in **2** is shown. The rest of the H atoms as well as counter ions and solvent molecules have been omitted for clarity.

Electrochemistry of 1-3 in organic media

The electrochemical properties of **2** and **3** were analyzed by cyclic voltammetry and spectroelectrochemical experiments in dimethylformamide (DMF) or acetonitrile (MeCN) and compared to those of the parent complex **1** under the same conditions (Figure 3, S1-S4 and Table S1). All complexes **1**-**3** feature two chemically reversible metal centered one-electron waves which were assigned to the $Co^{III/II}$ and $Co^{II/I}$ couples. Compounds **1** and **3** show basically the same reduction potential values at $E^1_{1/2}$= -0.37 V *vs* Fc^+/Fc (ΔE = 69-80 mV) and $E^2_{1/2}$= -0.88 V *vs* Fc^+/Fc (ΔE = 59-79 mV), respectively. In contrast, both electrochemical events show a significant anodic shift for compound **2**, suggesting that the penta-coordinated structure, with a neutral acetonitrile ligand in the axial position, observed in the solid state is also maintained in solution (E^1_a = 0.71 V and $E^{1\prime}_c$ = -0.04 V *vs* Fc^+/Fc (ΔE = 752 mV) for $Co^{III/II}$ and $E^2_{1/2}$= -0.71 V *vs* Fc^+/Fc (ΔE = 59 mV) for $Co^{II/I}$). The high peak to peak separation for the $Co^{III/II}$ couple, particularly for complex **2**, is associated with a square

mechanism involving ligand coordination, from square-based pyramid to octahedral geometry upon oxidation (Scheme S2). A third ligand based redox wave at $E^3_{1/2}$ ≈ -1.65 V *vs* Fc^+/Fc (ΔE = 70-110 mV) is observed for all the complexes, regardless of the substitution of the ligand on the amine group of the macrocyclic ligand. Compounds **1** and **3** show an additional irreversible oxidation wave at $E_{p,a}$≈ 0.85 V *vs* Fc^+/Fc due to the oxidation of chloride counter-anion to chlorine gas.[14]

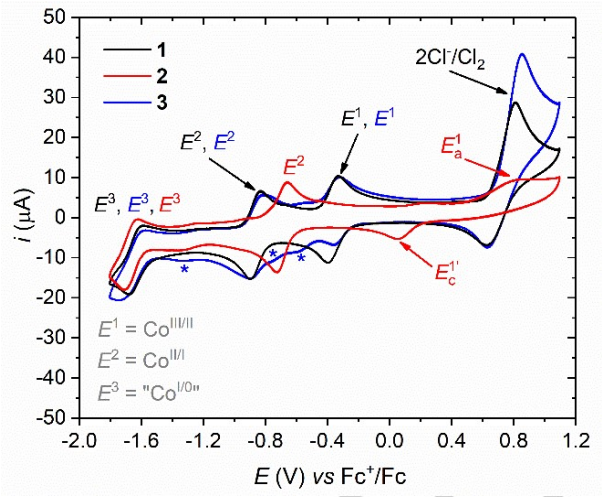

Figure 3. Second scan of a cyclic voltammetry experiment of compounds **1** (black), **2** (red) and **3** (blue) in DMF (0.1 M $[Bu_4N]PF_6$). E_i = open circuit potential. [Complex] = 1 mM; WE = Glassy Carbon disk; CE = Platinum disk; RE = $AgNO_3/Ag$ (converted to Fc^+/Fc by adding +0.096 V as determined experimentally); scan rate = 100 mV/s. Blue asterisks (*) indicate species derived from compound **3**, attributed to the formation of compound **4** in Figure 2 or related side-products).

Electrochemistry in aqueous media and hydrogen evolution electrocatalysis

The axial acetonitrile and chlorido ligands of **2** and **3** are exchanged by water in their aqueous solutions as demonstrated by UV-Vis spectroscopy experiments (Figure S5 and S6). The same substitution reaction has also been observed for **1** before.[13] Interestingly, the derivative compound **4** with the coordinated alkoxido group evolves to the same aqua complex derived from **3** in water due to the protonation of the alkoxido ligand in aqueous conditions (Figures S5 and S6).

Cyclic voltammetry experiments of **2** and **3** in pH 7 (See Figure 4 and Table 1) show a reversible $Co^{II/I}$ redox couple at the same potential, *i.e.*, $E_{1/2}$ = -0.51 V *vs* NHE (ΔE = 65-71 mV), which is 100 mV anodically shifted to that of **1** ($E_{1/2}$ = -0.61 V *vs* NHE (ΔE = 81 mV). These results suggest that in aqueous solution, **2** and **3** have the same coordination sphere at oxidation state +2, most likely a square-based pyramid with an aqua ligand in the axial position. In contrast, recent x-ray absorption spectroscopy experiments with compound **1** showed a pseudo-octahedral coordination sphere with an alongated Co-$O_{(axial)}$ bond.[13] This is in agreement with the shift of the $Co^{II/I}$ wave of **1** compared to those of **2** and **3**. A very broad, pH dependent wave associated with the $Co^{III/II}$ redox couple is also observed for compounds **1**-**3**, which is associated with a slow process involving significant rearrangements when changing the oxidation state of the Co center (see Scheme S2, Figure S7 and Table S2). Upon lowering the pH to 4.1, the $Co^{II/I}$ wave of **1** becomes irreversible due to the proton reduction catalysis, which is already described in detail in the literature (Figure 4, bottom left).[12,14] In sharp contrast, the $Co^{II/I}$ couples of **2** and **3** are almost fully reversible at this pH, indicative of the low reactivity of their Co^I derivatives. The reactivity of these Co^I species increases at pH 2, when all complexes show catalytic waves with similar shape (Figure 4, bottom right). Cyclic voltammetry experiments at variable scan rates show that catalyst **1** features a catalytic wave regardless of the scan rate (5-2000 mV/s). On the other hand, catalysts **2** and **3** show significant differences in the profile of the $Co^{II/I}$ wave upon changing the scan rate of the sweep. Thus, if the experiment is performed at sufficiently slow scan rate (5 mV/s) it is possible to observe a catalytic wave at pH 4.1 for both catalysts (Figures 5, dashed lines). In addition, when performing the experiment at a sufficiently fast scan rate (500 mV/s) at pH 4.1, it is possible to avoid the chemical reaction leading to catalysis and thus fully recover the reversibility of the $Co^{II/I}$ redox couple (Figure 5, solid lines).

The catalytic wave observed at the $Co^{II/I}$ couple of complexes **1**-**3** is associated with the formation of a Co^{III} hydride (Co^{III}-H) from the electrochemically generated Co^I (eq. 1). This hydride species is the gate to the hydrogen evolution catalytic cycle, and therefore a key intermediate, whose reactivity can determine the rate of the process.[19,20]

$$Co^I + H^+ \rightarrow Co^{III}\text{-}H \qquad \text{eq. 1}$$

Table 1 collects calculated pK_a values for the hexacoordinated Co^{III}-H intermediate with an aquo ligand in the axial position,

formed after protonation of a pentacoordinated Co^{I} species derived from **1**-**3** (see also Table S3 for additional data). They are all very acidic, indicating that the reaction depicted in eq. 1 is thermodynamically very demanding for the three catalysts.[19] These results are in agreement with the pH dependency of the catalytic response summarized in Figures 4 and 5 and invoke a catalytic mechanism where the formation of the Co^{III}-H, that is, the protonation of Co^{I}, is limiting the overall process at moderate pHs.[19,20] Analysis of the foot of the catalytic wave show a faster rate for **1** both in pH 4 and pH 2, despite the similarity on their respective pK_a (Figures 4, 5 and Figure S12). This is attributed to the different electronic environment around the cobalt metal center (hexacoordinated for **1** and pentacoordinated for **2** and **3**) as discussed above from the lower potential of the $Co^{II/I}$ couple in the cyclic voltammetry. The catalytic rates can also be strongly influenced by the lower rearrangement energy expected for the less hindered N-H group in **1** compared to **2** or **3** with bulkier N-CH_3 and N-CH_2-OH groups upon protonation (Scheme S2).

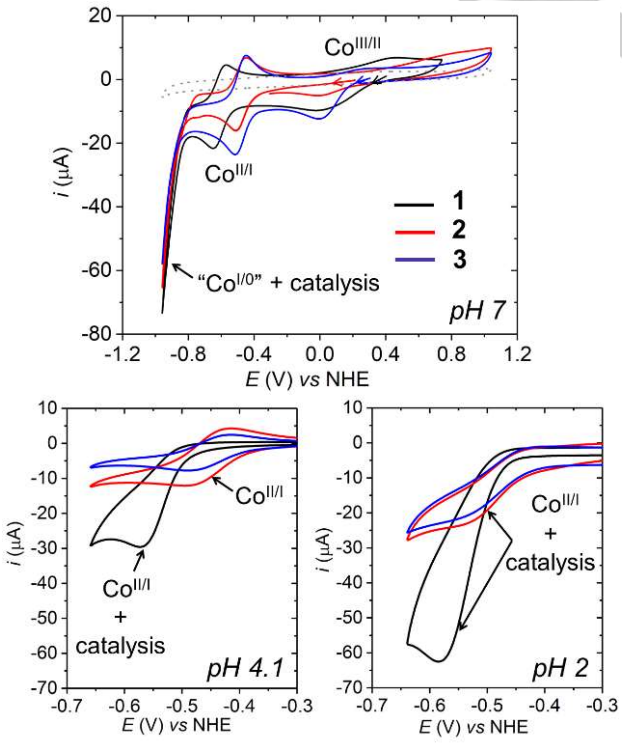

Figure 4. Cyclic voltammetry experiments in pH 7, pH 4.1 and pH 2 of **1** (black), **2** (red) and **3** (blue). Grey dashed lines correspond to the blank measurement. [Complex] = 1 mM; WE = glassy carbon disk; CE = Pt disk; RE = SCE (+0.241V vs NHE); scan rate = 100 mV/s.

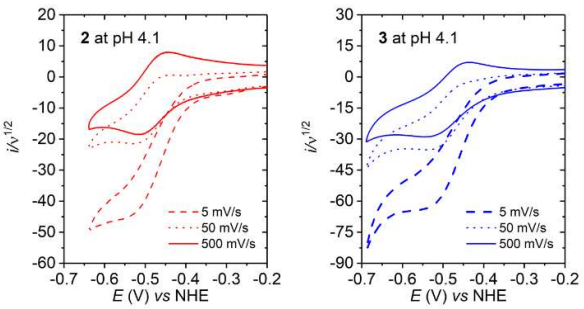

Figure 5. Cyclic voltammetry experiments in pH 4.1 at different scan rates for **2** (left) and **3** (right). [Complex] = 1 mM; WE = glassy carbon disk; CE = Pt disk; RE = SCE (+0.241V vs NHE); scan rate = 100 mV/s.

Hydrogen Evolution photocatalysis

The photochemical water reduction activity of catalysts **2** and **3** was carried out in a thermostated 4 mL photoreactor at 25°C using $[Ru(bpy)_3][ClO_4]_2$ as photosensitizer and a 1:1 mixture of ascorbic acid/sodium ascorbate as sacrificial electron donor and buffer at pH 4.1. A Xe lamp equipped with a UV light filter provided the light source calibrated to 1 sun intensity. The hydrogen gas evolution was monitored with a Clark electrode. The profiles are shown in Figure 6, as well as the profile of reported catalyst **1** measured under the same experimental conditions for comparison purposes. Under photochemical conditions, the three catalysts show similar rates as deduced from the slopes of the hydrogen evolution profiles. Compound **2** is the fastest catalyst with an initial turnover frequency (TOF_i) of 0.15 s^{-1} and a turnover number (TON) of 466 (Figure 6, red trace). Catalyst **3** has a similar catalytic rate but deactivates in less than 1h of reaction (Figure 6, blue trace, TOF_i = 0.11 s^{-1}, TON = 168). We attribute the fast deactivation of **3** to the interaction of the dangling hydroxymethyl group that can intra or intermolecularly coordinate the cobalt center, as proven by the species **4** and **5** isolated in reaction mixtures during the synthesis of **3**. As a consequence,

inactive mono and polynuclear species may form and stop the catalysis. Interestingly, catalyst **1** is the slowest with TOF_i = 0.09 s^{-1} but the most stable catalyst (Figure 6, black trace, TON = 680). This result is in contrast to the relative catalytic rates observed under electrochemical conditions in Figure 4 and Figure S11, which clearly show that **1** is the fastest.

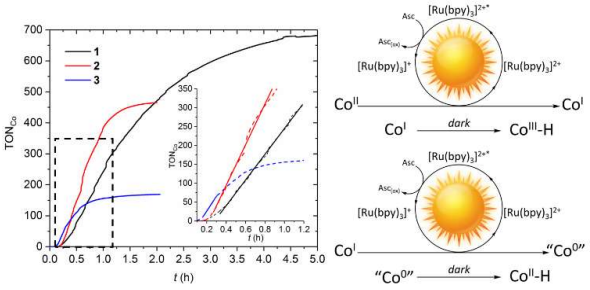

Figure 6. Hydrogen evolution photocatalysis in acidic water. [Cat] = 0.05 mM; $[Ru(bpy)_3]^{2+}$= 0.5 mM; [ascorbic acid] = [sodium ascorbate] = 0.55 M; pH = 4.1. Light intensity calibrated to 1 sun illumination, 100 mW/cm^2. TON_{Co} = turnover number = mols of H_2/mols of cobalt catalyst.

Mechanistic insights from experimental and computational studies

While electrocatalysis at the $Co^{II/I}$ couple unambiguously determines the protonation of the Co^{I} intermediate as the rate determining step (rds) of the process, it is not obvious in the case of the photochemical reaction at pH 4.1, in which the relative kinetics of catalysts **1**-**3** follow a different trend. Thus, a different mechanistic pathway must be responsible for the hydrogen evolution reaction under photocatalytic conditions. Over the course of the bulk photochemical experiments, sufficient reductive equivalents provided by photogenerated $[Ru(bpy)_3]^{+}$ are available (initial ratio [Co]:[Ru] is 1:10) such that a second reduction of the initial complex to generate a formal "Co^{0}" species can reasonably take place (Figure 6, right). "Co^{0}" species refers to a reduced species where the additional electron is shared between ligand and metal center as indicated by spin population analysis (Table S12). Indeed, the reduction potential of the $[Ru(bpy)_3]^{2+}$/$[Ru(bpy)_3]^{+}$ couple is about 80 mV lower than the second reduction of complexes **1**-**3** as indicated by their respective cyclic voltammetry experiments in organic solvents ($E_{1/2}$ = -1.73 V and $E_{1/2}$ ≈ -1.65 V *vs* Fc^{+}/Fc respectively, see Figures 3 and S12). Although these values prove the feasibility of the electron transfer, they do not provide any information about its kinetics. A thorough time-resolved spectroscopic analysis should be carried out to fully understand the charge transfer dynamics responsible of the generation of the "Co^{0}" species.[13,14]

The basicity of the doubly reduced species "Co^{0}" is obviously much higher than the analogous Co^{I} derivative. This is quantified by DFT in an increase of approx. 20 orders of magnitude in the relative acidities of the corresponding hydrides as indicated in Table 1.

DFT calculations were also employed to study different potential intermediate species involved in the hydrogen evolution catalysis as well as transition states (TS) of the intermolecular H-H bond formation step for catalysts **1**-**3**. In addition, a TS derived from an intramolecular pathway involving the N-H group was also calculated for catalyst **1**, which is the only compound with an available proton-like group in close proximity to the cobalt hydride. Finally, a third family of TS was considered where a putative protonated amine group H-N^{+}-R is involved in the hydrogen formation step (R = H, CH_3 or CH_2OH for **1**, **2** and **3** respectively). All geometry optimizations were performed using the BP86 exchange-correlation functional[21,22] and all reported energies correspond to free energies that were obtained using also the B3LYP-D3/def2-TZVP/COSMO level of theory (see details in the supporting information).[23,24,25] The flexible nature of the tetraazamacrocyclic equatorial ligand and labile axial positions in **1**, **2** and **3** offer a high degree of complexity to the studied systems allowing for different coordination numbers depending on the cobalt oxidation state as well as different relative disposition of the N-R group with respect to the axial ligands, where R = H, CH_3 or CH_2OH for **1**, **2** and **3** respectively. This is illustrated for the four optimized structures related to a putative Co^{III} hydride intermediate derived for **1** in Figure 7. In order to obtain a complete picture of the plausible intermediates and mechanistic pathways, all the possibilities were considered in our calculations as described in detail in the supporting information.

Table 1 collects the theoretical reduction potentials of the $Co^{II/I}$ couple in the range of $E_{1/2}(Co^{II/I})_{calc}$ = -0.61 to -0.55 V that match well with the experimental values ($E_{1/2}(Co^{II/I})_{exp}$ = -0.61 to -0.51 V). We find that the reduction potential of the Co^{III}-H intermediate to give a reduced Co^{II}-H is more positive than the $Co^{II/I}$ couple for the three catalysts as expected, suggesting that once the Co^{III}-H is generated, it is immediately reduced ($E_{1/2}(Co^{III/II}\text{-H})_{calc}$ = -0.11 to -0.01 V, Table 1 and Table S3). The hydrogen evolution reaction mechanism via Co^{II}-H has already been previously proposed for catalyst **1** under electrochemical conditions.[11]

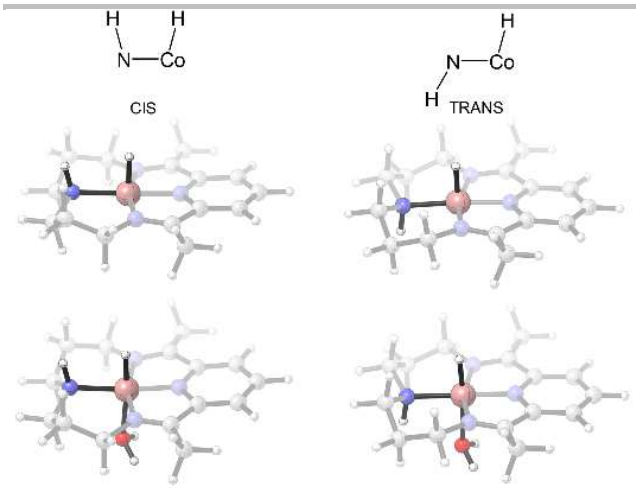

Figure 7. DFT optimized structures of a Co^{III}-H species derived from **1**. Top: pentacoordinated species, cis and trans. Bottom: hexacoordinated species: cis and trans.

A model system using four hydrogen bonded water molecules was used to calculate the transition states for the intermolecular H-H bond formation with catalysts **1**-**3** from Co^{II}-H (Figure 8, left). Two cobalt species were considered, one with square based pyramid and one with octahedral geometry containing an additional aquo ligand. Similar trends were observed for the two families of compounds and thus we will restrict our discussion to the penta-coordinated species, which gives the lowest barriers. In all the cases the N-R group (R = H, CH_3 or CH_2OH for **1**, **2** and **3** respectively) is in trans relative position to the hydrido ligand in the Co^{II}-H species. As depicted in the left of Figure 8, the kinetic barriers to form hydrogen from the Co^{II}-H with this model are around $\Delta G^{\neq}$ = 18 kcal/mol.

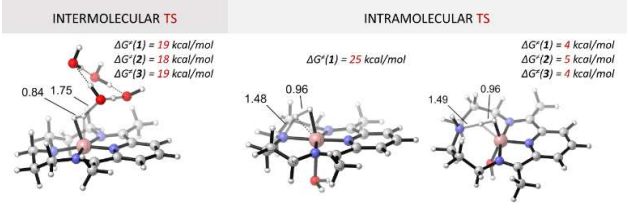

Figure 8. Intermolecular vs intramolecular H-H bond formation. Transition states (TS) relevant to the hydrogen evolution reaction by catalysts **1**-**3**. The kinetic barriers ($\Delta G^{\neq}$) are indicated for each catalyst in kcal/mol and representative drawings of each TS is given for **1**. $\Delta G^{\neq}$ = G(TS) - G(Co^{II}-H), see more details in the supporting information.

These values cannot distinguish catalytic rates between the three catalysts as they are essentially the same if one considers the inherent error of the calculations. Importantly, these results are consistent with the relatively similar slopes of the hydrogen evolution profiles obtained in the photochemical reactions of Figure 6 if we consider the H-H bond formation as the rds. On the other hand, the intramolecular pathway involving the N-H group of **1** requires a much higher energy in the range of 24.8 to 30.0 kcal/mol depending on the coordination number (5 or 6) and oxidation state of the cobalt (II or III), ruling out this catalytic pathway (Figure 8, middle and Table S6). In addition, we should emphasize here that the isomers with a relative cis configuration of the N-H group in regards to the hydrido group in Co^{II}-H are 1-2 kcal/mol higher in energy than the corresponding trans counterparts. Interestingly, an intramolecular pathway involving a protonation of the amine in the macrocyclic ligand resulted in lower kinetic barriers for the three catalysts ($\Delta G^{\neq}$ = 4-5 kcal/mol, Figure 8 right and Table S8). However, this path is not likely because the energy of the previous step involving amine protonation and decoordination is in the range of 20-35 kcal/mol (Figure S12, Tables S9 and S10). Thus, the most favorable path involves an intermolecular H-H bond formation between the Co^{II}-H and an incoming water molecule.

Summary and Conclusions

A thorough analysis of the hydrogen evolution catalytic behavior of **1**, **2** and **3** shows the intricate role of the macrocyclic ligand that occupies the equatorial position of this family of Co catalysts. First of all, the bulkiness and electronic properties of the substituent on the amine group of the macrocyclic frame determines the geometry and electronic density on the metal center as demonstrated by XRD studies summarized in Figure 2 and electrochemical properties in Figures 3 and 4. These changes have consequences in the pK_a of the cobalt hydride species and the kinetics of the formation of these key intermediates towards the hydrogen evolution reaction. In those catalytic systems where the Co^{III}-H is involved, the protonation step from Co^{I} to Co^{III}-H is the rds of the overall process, dictated by the low pK_a of the hydrides as illustrated in the left of Scheme 1. This has been

unambiguously proven by cyclic voltammetry experiments, for instance at pH higher than 2 where the concentration of protons is limited and the catalysis by **2** and **3** is hindered.

In sharp contrast, this is not the case in photo induced catalysis under continuous light irradiation using $[Ru(bpy)_3][ClO_4]_2$ as photosensitizer, which after photoactivation and reductive quenching by the ascorbate, has enough reducing power to generate a doubly reduced "Co^0" species (Scheme 1, right). The latter can be protonated to form the corresponding Co^{II}-H species, which have a much higher pK_a compared to that of its Co^{III}-H counterpart (Table 1). In this scenario, the H-H bond formation is the rds.

Table 1. Reduction potentials for the $Co^{II/I}$ and $Co^{III/II}$-H couples in aqueous conditions and pK_a values of the cobalt hydride species. See supporting information for details regarding the DFT calculations.

Catalyst	$E(Co^{II/I})$[a]		$E(Co^{III/II}\text{-H})$[a]	pK_a[18] $(Co^{n+} - H \rightleftharpoons Co^{(n-2)+} + H^+)$	
	Exp.[b]	Calc.[c]	Calc.[d]	Co^{III}-H[e]	Co^{II}-H[e]
1	-0.61 (ΔE = 71 mV)	-0.61	-0.06	-1.5	12.0
2	-0.51 (ΔE = 65 mV)	-0.61	-0.11	-2.7	12.5[f]
3	-0.51 (ΔE = 71 mV)	-0.55	-0.01	-3.6	11.8[f]

[a] *Potentials reported in Volts vs NHE. [b] Values correspond to the $E_{1/2}$ values obtained from cyclic voltammetry experiments at pH 7 where no catalysis is observed, in parenthesis ΔE indicates the peak to peak separation between $E_{p,c}$ and $E_{p,a}$ waves. [c] DFT calculated values for the reduction of the penta-coordinated cobalt species with an aquo ligand in the axial position in cis orientation relative to the N-R group (R = H, **1**; R = CH_3, **2**; R = CH_2OH, **3**). [d] DFT calculated values for the penta-coordinated cobalt species with an hydrido ligand in the axial position in trans orientation relative to the N-R group (R = H, **1**; R = CH_3, **2**; R = CH_2OH, **3**). [e] DFT calculated values for the octahedral cobalt species with aqua and hydrido ligands in the axial positions, the latter in trans orientation relative to the N-R group (R = H, **1**; R = CH_3, **2**; R = CH_2OH, **3**) to give a penta-coordinated cobalt species upon proton loss. See supporting information for details and complementary data.*

A series of plausible transition states involving intermolecular as well as intramolecular pathways have been calculated. The flexibility and different relative positions (cis or trans) of the substituent in the amine group of the macrocyclic ligand offers a high degree of complexity to the studied system. After analysis of different possibilities, two different mechanisms with Co^{II}-H key intermediates are proposed to contribute to the hydrogen evolution catalysis by **1**, **2** and **3** (Scheme 1, right). The first one involves intermolecular H-H bond formation between the cobalt hydride and one proton of an incoming water molecule, which has the lowest activation barrier according to our calculations (17-19 kcal/mol). The second one consists in the intramolecular interaction between an ammonium proton in the macrocyclic ligand and the cobalt hydride, with a higher energy demand caused by the formation of the reactive ammonium intermediate, which requires decoordination of the amino ligand and significant rearrangement of the molecule (17-25 kcal/mol). The activation energies in both catalytic pathways do not differ significantly within the three complexes. These calculations are in full agreement with the experimental photocatalytic results that show similar slopes for the hydrogen evolution profiles in Figure 6.

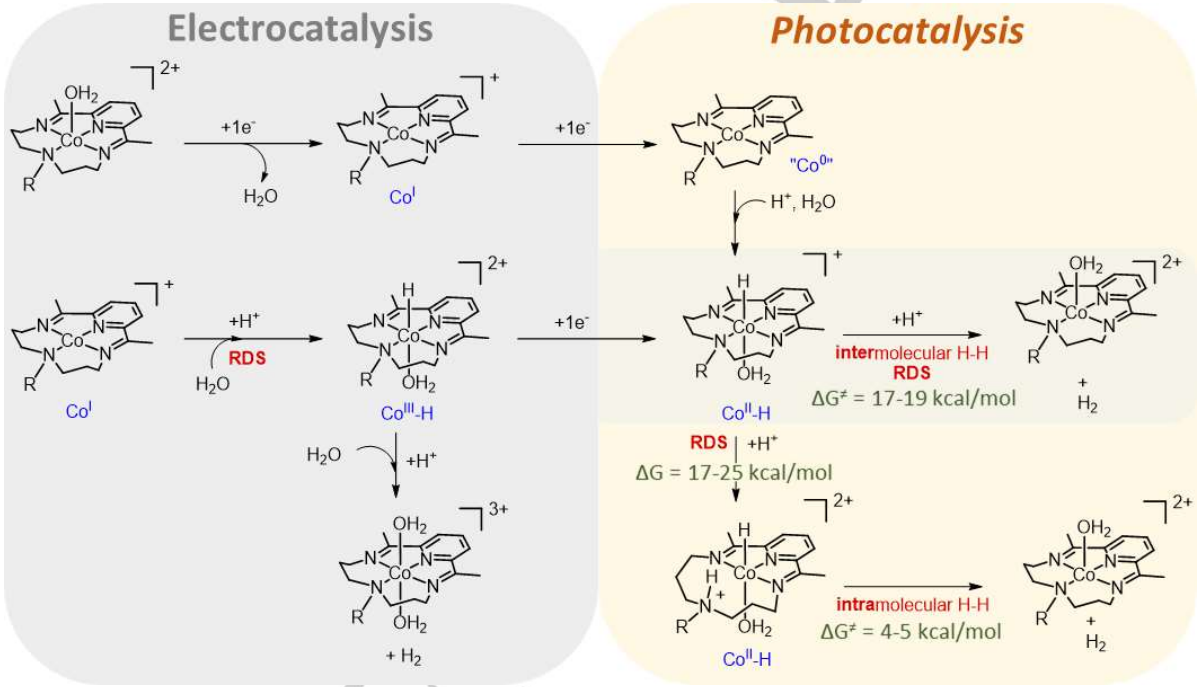

Scheme 1. Catalytic pathways towards hydrogen evolution by catalysts **1-3**. RDS: rate determining step of the process.

Experimental Section

Reagents: All organic reagents, salts for buffers and metal precursors were purchased from Sigma-Aldrich and used without further purification. Anhydrous solvents were taken from a solvent purification system (SPS®). Compound **1** was prepared following an adapted reported procedure,[11] details are given in the supporting information.

Electrochemistry methods and equipment: Glassy carbon (GC) disk electrodes, Platinum disk electrodes and reference electrodes (SCE and $AgNO_3$/Ag) were purchased from IJ-Cambria Ldt. Pads and alumina for polishing were also purchased from the same company. Buffer solutions at pH 7 and pH 2 were prepared with Na_2HPO4, NaH_2PO4 and adjusted to 0.1 M ionic strength. Buffer solutions at pH 4.1 were prepared with ascorbic acid:sodium ascorbate mixtures 1:1 (0.55 M). Cyclic voltammetry experiments were performed with a CHI660D potentiostat in a one-compartment cell, three electrode system using GC disk as working electrode, platinum disk as counter electrode and standard calomel electrode (SCE) or $AgNO_3$/Ag reference electrodes. **Spectroelectrochemistry:** Experiments were performed in a custom-made Optically Transparent Thin Layer Electrochemical (OTTLE) cell (University of Reading) with platinum mesh working electrode, platinum wire counter electrode and silver wire pseudo-reference electrode. **UV-vis equipment:** UV-Vis measurements were carried out on a Lambda 1050 PerkinElmer spectrophotometer equipped with a PMT, InGaAs and PbS detectors system, double beam optics, double monochromator and D2 and W light sources.

Preparation of 2: 2,6-diacetyl-pyridine (326.4 mg, 2 mmol) and $Co(NO_3)_2 \cdot 6H_2O$ (582.06 mg, 2 mmol) were dissolved in degassed anhydrous methanol (10mL), heated to 75°C under N_2 and the reaction mixture stirred until everything was dissolved, giving a pink-red solution. 3,3-Diamino-*N*-methyldipropylamine (0.32 mL, 2 mmol) was added dropwise. The solution turned dark and cloudy upon addition of the amine. Glacial acetic acid (0.1 mL) was added to catalyze the imine condensation, forming a clear solution. The reaction mixture (dark red) was stirred and kept at

75°C for 5 hours under N_2. After 5 hours, the condensation was complete. The reaction mixture was cooled down to room temperature, filtered under N_2 and transferred into a Schlenk flask containing a degassed methanolic solution of $NaClO_4$ (561.8 mg, 4 mmol). After a second filtration to remove a white solid, the filtered solution was dried under reduced pressure and redissolved in degassed anhydrous acetonitrile. An orange powder precipitated by adding degassed diethylether to the acetonitrile solution (729 mg). The product was recrystallized dissolving the powder in acetonitrile (40 mL) and layering toluene on top very slowly (40 mL). After 2-4 hours, dark orange crystals of compound **2** were obtained. The crystals were filtered under air and washed with toluene (522.3 mg, 0.914 mmol, 46%). Single crystals were obtained by slow diffusion of diethylether into an acetonitrile solution of **2**. Anal. Calcd for $C_{18}H_{27}Cl_2CoN_5O_8$: C, 37.84; H, 4.76; N, 12.26. Found: C, 37.80; H, 4.36; N, 12.30. ESI$^+$-HRMS m/z: calcd for $[M\text{-}CH_3CN]^+$ ($C_{16}H_{24}CoN_4^+$): m/z: 331.1333, found m/z: 331.1332. *Note: the use of perchlorate salts may lead to explosive mixtures and therefore they should be handled with caution and in small quantities.*

Preparation of 3, 4 and 5: 2,6-Diacetyl-pyridine (686 mg, 4.2 mmol) and $CoCl_2{\cdot}6H_2O$ (1 g, 4.2 mmol) were dissolved in degassed ethanol (6.3mL) and heated to 75°C under N_2 (deep blue solution). Degassed water (4.2 mL) was added and the mixture was stirred until everything was dissolved, giving a purple solution. 3,3-Diamino-*N*-methyldipropylamine (0.7 mL, 4.2 mmol) was added dropwise. The solution turned to dark blue and cloudy on addition of the amine. Glacial acetic acid (0.2 mL) was added to catalyze the condensation giving a clear solution, which was stirred and kept at 75°C for 5 hours under N_2. At this point, the reaction mixture became dark red. After 5h, the condensation was judged to be complete and the mixture was cooled down to room temperature. A concentrated HCl aqueous solution (0.39 mL, 37 %, 4.62 mmol,) was added. The mixture was aerated overnight. The reaction mixture was dried under reduced pressure and the resulting solid was dissolved in the minimum volume of methanol (brown solution). Green solid precipitated when isopropanol was added dropwise. The solid was filtered and washed with isopropanol. The green powder was dissolved in water and acetone was added until the solution started to become cloudy. Then the solution was kept in the fridge overnight. The green solid was filtered and identified as compound **4** containing traces of compound **3** (572 mg, *ca.* 1.2 mmol, *ca.* 30%). Single crystals of **4** were obtained by slow diffusion of diethylether in a solution of **4** in methanol. ^{1}H NMR (500 MHz, D_2O-d_2) δ = 8.53 (dd, J = 8.4 and 7.3 Hz, 1H), 8.46 (d, J = 7.9 Hz, 2H), 5.27 (s, 2H), 4.21 (dt, J = 15 and 3.2 Hz, 2H), 3.81 (t, J = 13.7 Hz, 2H), 3.51 (td, J = 12.85 and 2.6 Hz, 2H), 2.9 (s, 6H), 2.76 (dt, J= 12.9 and 3.1 Hz, 2H), 2.55-2.37 (m, 4H). ^{13}C NMR (126 MHz, D_2O-d_2) δ =178.8, 157.7, 142.6, 127.8, 90.8, 56.1, 49.5, 24.9, 16.9. ESI$^+$-HRMS m/z: calcd for $[M]^+$ ($C_{16}H_{23}ClCoN_4O^+$): m/z: 381.0892. Found m/z: 381.0887. **Compound 3** was prepared by adding 10 equivalents of hydrochloric acid to an aqueous solution of **4**. Dark green microcrystals can be obtained by adding acetone to the acidic mixture and cooling it down to -20ºC overnight. Single crystals were obtained by slow diffusion of diethylether in a solution of **3** in methanol. ^{1}H NMR (400 MHz, MeOD-d_4) δ = 8.49 (t, J = 8.0 Hz, 1H), 8.40 (d, J = 8.0 Hz, 2H), 4.60 (s, 2H), 3.96 (m, 2H), 3.64 (m, 2H), 3.54 (t, J=12.5 Hz, 2H), 3.14 (dq, J=3.5, 1.5 Hz 2H), 2.81 (s, 6H), 2.35 (m, 2H), 2.10 (m, 2H). ^{13}C NMR (101 MHz, MeOD-d_4) δ = 179.6, 157.2, 141.5, 127.6, 82.5, 51.3, 50.4, 22.0, 16.7. Anal. Calcd for $C_{16}H_{24}Cl_3CoN_4O$: C, 42.36; H, 5.33; N, 12.35. Found: C, 41.19; H, 5.51; N, 12.14. ESI$^+$-HRMS m/z: calcd for $[M\text{-}H,Cl]^+$ ($C_{16}H_{23}ClCoN_4O^+$): m/z: 381.0892, found m/z: 381.0887 (**3** converts into **4** in the MS chamber). Single crystals of **Compound 5** were isolated from the methanolic solution of the first filtration during the synthesis of **4** described above. We attribute the formation of **5** to the presence of excess of $CoCl_2$. ^{1}H NMR (400 MHz, MeOD-d_4) δ = 8.53 (t, J = 7.8 Hz, 1H), 8.45 (d, J = 7.8 Hz, 2H), 5.30 (s, 2H), 4.20 (m, 2H), 3.81 (m, 2H), 3.52 (m, 2H), 2.89 (s, 6H), 2.75 (m, 2H), 2.56-2.36 (m, 4H). We attribute the broad bands observed in the ^{1}H NMR spectrum to the Co^{II} atom (particularly for the -CH_2- group, the closest to the paramagnetic center). Anal. Calcd for $C_{16}H_{23}Cl_4Co_2N_4O$: C, 35.13; H, 4.24; N, 10.24. Found: C, 35.18; H, 3.98; N, 10.14.

General procedure for photochemical experiments: In a 20 mL glass vial, a mixture of solid acorbic acid (284.0 mg, 1.6 x 10^{-3} mol) and sodium ascorbate (326.9 mg, 1.6 x 10^{-3} mol) was added to a 2.9 mL aqueous solution containing $[Ru(bpy)_3](ClO_4)_2$ (5.17 x 10^{-4} M). The mixture was sonicated and protected from the light until all the salts were dissolved. The solution was transferred in a water-jacketed 4 mL flask and 0.1mL of cobalt catalyst (**1**, **2** or **3**) were added (1.5 x 10^{-3} M) reaching a final composition of 0.55M of ascorbic acid and sodium ascorbate, 0.05 mM of cobalt catalyst and 0.5 mM of ruthenium photosensitizer. The flask was sealed with a septum and the mixture degased for 1 hour by bubbling nitrogen. A Clark hydrogen sensor was inserted in the cell and the mixture irradiated using a 150 W Xe Arc Lamp with a cut off filter (λ > 400 nm, 25 mm). The light intensity was calibrated to "1 sun" previous to the experiment and the temperature was maintained constant at 25 ºC. At the end of the experiment, the cell was degased with nitrogen and calibrated adding known amounts of hydrogen.

Acknowledgements

Support from MINECO, FEDER and AGAUR are gratefully acknowledged through grants CTQ2016-80058-R, CTQ2015-73028-EXP, SEV 2013-0319, ENE2016-82025-REDT, CTQ2016-81923-REDC, and 2017-SGR-1631. The work has further been supported by the University of Zurich, the University Research Priority Program „Solar Light to Chemical Energy Conversion" (LightChEC) and the Swiss National Science Foundation (grant. No. PP00P2_170667). Computational time by the Swiss national supercomputing center (accounts: s745 and s875) are gratefully acknowledged.

Keywords: hydrogen evolution • cobalt • macrocyclic ligand • mechanism • catalysis

[⊥] Current address: Instituto Madrileño de Estudios Avanzados en Nanociencia (IMDEA-Nanociencia), Calle Faraday 9, 28049, Madrid, Spain

[1] J. R. McKone, N. S. Lewis, H. B. Gray, H. B. *Chem. Mater.* **2014**, *26*, 407–414.
[2] N. S. Lewis, *Science* **2016**, *351*, 353–364.
[3] P. Du, R. Eisenberg, *Energy Environ. Sci.* **2012**, *5* (3), 6012–6021.
[4] W. T. Eckenhoff, R. Eisenberg, R. *Dalt. Trans.* **2012**, *41*, 13004–13021.
[5] S. Berardi, S. Drouet, L. Francàs, C. Gimbert-Suriñach, M. Guttentag, C. Richmond, T. Stoll, T.; A. Llobet, *Chem. Soc. Rev.* **2014**, *43*, 7501–7519.
[6] V. Artero, J. M. Saveant, *Energy Environ. Sci.* **2014**, *7*, 3808–3814.
[7] R. S. Khnayzer, V. S. Thoi, M. Nippe, A. E. King, J. W. Jurss, K. A. El Roz, J. R. Long, C. J. Chang, F. N. Castellano, *Energy Environ. Sci.* **2014**, *7*, 1477–1488.
[8] V. Artero, M. Chavarot-Kerlidou, M. Fontecave, *Angew. Chem. Int. Ed.* **2011**, *50*, 7238.
[9] M. L. Helm, M. P. Stewart, R. M. Bullock, M. R. DuBois, D. L. DuBois, *Science* **2011**, *333*, 863–866.
[10] C. C. L. McCrory, C. Uyeda, J. C. Peters, *J. Am. Chem. Soc.* **2012**, *134*, 3164–3170.
[11] C. F. Leung, Y.-Z.Chen, H.-Q.Yu, S.-M.Yiu, C.-C. Ko, T.-C. Lau, T *Int. J. Hydrogen Energy* **2011**, *36*, 11640–11645.
[12] F. Molton, J. Fortage, A. Deronzier, A. G. Blackman, T. Stoll, M.-N. Collomb, S. Varma, C. E. Castillo, *Phys. Chem. Chem. Phys.* **2013**, *15*, 17544–17552.
[13] D. Moonshiram, C. Gimbert-Suriñach, A. Guda, A. Picon, C. S. Lehmann, X. Zhang, G. Doumy, A. M. March, J. Benet-Buchholz, A. Soldatov, A. Llobet, S. H. Southworth, *J. Am. Chem. Soc.* **2016**, *138*, 10586–10596.
[14] C. Gimbert-Suriñach, J. Albero, T. Stoll, J. Fortage, M.-N. Collomb, A. Deronzier, E. Palomares, A. Llobet, *J. Am. Chem. Soc.* **2014**, *136*, 7655–7661.
[15] M. Sandroni, R. Gueret, K. D. Wegner, P. Reiss, J. Fortage, D. Aldakov, M.-N. Collomb, *Energy Environ. Sci.* **2018**, *11*, 1752–1761.
[16] R. Gueret, L. Poulard, M. Oshinowo, J. Chauvin, M. Dahmane, G. Dupeyre, P. P. Lainé, J. Fortage, M.-N. Collomb, *ACS Catal.* **2018**, *8*, 3792–3802.
[17] C.-K. Poon, S. S. T. Liao, *J. Chem. Soc. Dalt. Transitions* **1978**, 1180–1185.
[18] D. C. Lacy, C. C. L. McCrory, J. C. Peters, *Inorg. Chem.* **2014**, *53*, 4980–4988.
[19] R. H. Morris, *Chem. Rev.* **2016**, *116*, 8588–8654.
[20] M. Natali, ACS Catal. **2017**, 7, 1330–1339
[21] A. D. Becke, *Phys. Rev. A* **1988**, *38*, 3098–3100.
[22] J. P. Perdew, *Phys. Rev. B* **1986**, *33*, 8822–8824.
[23] F. Weigend, R. Ahlrichs, *Phys. Chem. Chem. Phys.* **2005**, *7*, 3297–3305.
[24] S. Grimme, J. Antony, S. Ehrlich, H. A. Krieg, *J. Chem. Phys.* **2010**, *132*, 154104.
[25] A. Klamt, G. Schuurmann, G. *J. Chem. Soc. Perkin Trans* **1993**, *2*, 799–805.

WILEY-VCH

RESEARCH ARTICLE

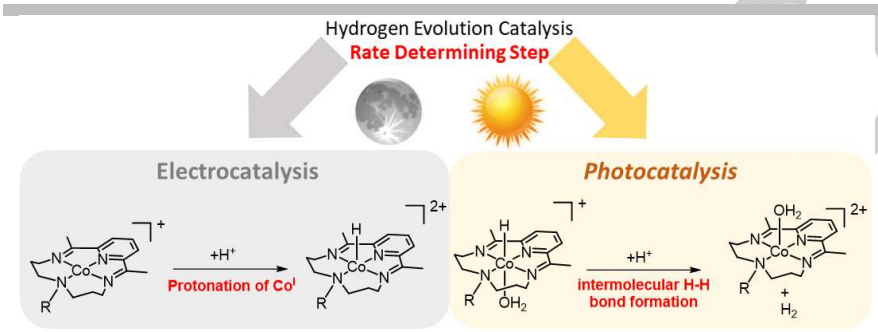

A study of the hydrogen evolution catalysis by cobalt complexes bearing a tetraazamacrocyclic ligand show that the relative rates and mechanistic pathways are dependent on the catalytic conditions. Under electrochemical driven catalysis the rate determining step (RDS) is the protonation of the Co^{I} intermediate while the intermolecular H-H formation step is the RDS for photochemical induced reactions using $[Ru(bpy)_3]^{2+}$ as photosensitizer.

Sergi Grau, Mauro Schilling, Dooshaye Moonshiram, Jordi Benet-Buchholz, Sandra Luber, Antoni Llobet* and Carolina Gimbert-Suriñach**

Page No. – Page No.

Electrochemically and Photochemically Induced Hydrogen Evolution Catalysis with Co-Tetraazamacrocycles Occur via Different Pathways